15th Triennial World Congress, Barcelona, Spain

CONSTRUCTION OF NAVIGATION AND CONTROL SYSTEMS OF A LARGE-SCALE UNMANNED HELICOPTER BASED ON IDENTIFIED MODEL

Seiji Hashimoto [*,1] **Shuichi Adachi** [**] **Yasunobu Segawa** [**]
Gou Miyamori [***] **Takeshi Akasaka** [***] **Anzhong Tan** [***]

[*] *Gunma University, Japan*
[**] *Utsunomiya University, Japan*
[***] *Kawada Industries, Inc., Japan*

Abstract: In this paper, first, system identification experiments for a large-scale unmanned helicopter are carried out to obtain a mathematical model of aircraft dynamics. The attitude error of the helicopter is compensated by a stability augmentation system (SAS) that permits the experiments during the flight. System identification results are shown on the dynamics by using the measured input and output data. Next, GPS (Global Positioning System) and INS (Inertial Navigation System) hybrid navigation system which obtains a present aircraft's information is discussed. Moreover, the robust position control system based on the identified mathematical model of aircraft is constructed. Finally, the position control experiments suggest that the proposed modeling and design approach is effective enough for practical applications.

Keywords: Helicopter control, Autonomous control, System identification, Navigation systems, Robust control

1. INTRODUCTION

Recently, unmanned helicopters, particularly large-scale ones, have been expected not only for the industrial fields such as agricultural spraying and aerial photograph, but also for such fields as observation, rescuing, and fire fighting. For these monotonous or dangerous missions, an autonomous flight control of the helicopter is indispensable. The autonomous flight control requires integrating technologies such as trouble diagnosis and obstacle avoidance as well as attitude and position controls.

The flight control of the helicopter involves some difficulties due to the following;

- The dynamics of the helicopter is essentially unstable.
- The characteristic values in the dynamics are usually nonlinear with air speed.
- The helicopter has six degrees of freedom in its motion (up/down, fore/aft, right/left, rolling, pitching, yawing).
- The helicopter is a multi-input multi-output system.
- Flight modes are cross-coupled.
- The flight is strongly affected by disturbances such as wind, temperature, etc.

The helicopter, however, can be modeled as a linear system around the trim points, i.e., a flight with no accelerations and no moments. Moreover, the system can be stabilized by using a SAS, which can also reduce the influence of cross-couple terms. Therefore, the flight control of the unmanned helicopter with SAS is possible

[1] Partially supported by the Grant-in-Aid for Scientific Research from JSPS

around the trim points. Several unmanned helicopters have been developed(Nguyen and Prasad, 1999),(Kobayashi and Liu, 1997), or are under development throughout the world.

The goal of the research is to design an autonomous flight control system of a large-scale unmanned helicopter. The purposes of this paper are to derive the mathematical model of the full-scale unmanned helicopter via system identification experiments, to construct the GPS/INS hybrid navigation system in order to obtain a present aircraft's position, and to design a robust position control system based on the identified model.

2. A LARGE-SCALE UNMANNED HELICOPTER

The configuration of an autonomous flight control of a large-scale unmanned helicopter is shown in Fig. 1. The flight control of the body is accomplished by using various sensors, which are represented by GPS, in accordance with the command reference transmitted by the ground station. The signals that lack for the autonomous flight can be estimated by the on-board digital signal processor (DSP). The control algorithm for the flight is installed in the DSP in advance. In addition, stabilization of the helicopter is realized by the SAS installed in the DSP. Thus the unmanned helicopter can be remotely controlled on the ground station. This experiment is devised so that a remote operator can transmit a rudder modification signal directly to the flight control in order to keep the flight safe.

The full-scale unmanned helicopter (RoboCopter) developed by Kawada Industries, Inc.(G. Miyamori and Hirai, 1997) is shown in Fig.2. The size and performance of the helicopter are summarized in Table 1. This unmanned helicopter is a remodeled version of a manned helicopter, Shweizer 300CB.

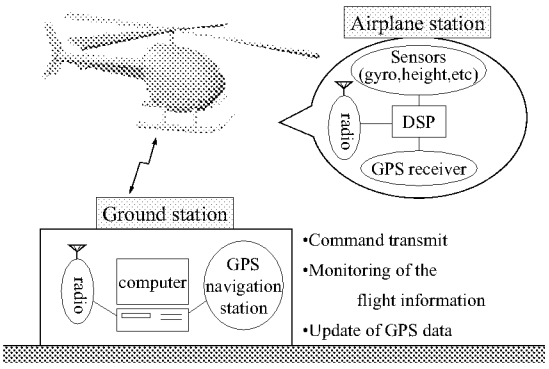

Fig. 1. Configuration of an autonomous flight system

Fig. 2. The experimental large-scale unmanned helicopter named RoboCopter

Table 1. Size and performance of RoboCopter

body dimensions	length	7.31 m
	width	1.99 m
	height	2.65 m
weight	total weight	794 kg
	empty weight	500 kg
	payload	294 kg
engine	type	air-cooled 4-cycle engine
	power	124 kW (168HP)
main rotor	number of blades	3
	diameter	8.18 m
tail rotor	number of blades	2
	diameter	1.30 m
continuous flight time	100 min (extendable to 4 h depending on payload)	

3. MODELING OF THE HELICOPTER

3.1 *System identification experiments*

The command signals, which are made in the computer on the ground station are transmitted to the helicopter. Modification rudder signals from the remote operator are added to these signals and then fed to the SAS controller for the attitude control. These input signals $\theta_C^{cmd}, \theta_S^{cmd}, \theta_{0T}^{cmd}$ and θ_{0M}^{cmd} drive rolling, pitching, yawing and heaving motions, respectively. The superscript (cmd) represents the reference value of those signals. $\theta_C^{cmd}, \theta_S^{cmd}, \theta_{0T}^{cmd}$ and θ_{0M}^{cmd} are used as input signals for system identification. In this case, taking the cross-couplings into consideration, each motion was separately excited by the signals. The pseudo random binary signal (PRBS) was applied to a motion of interest, and the constant signals were applied to the other three motions. The sampling time for the experiment was 0.05 s, and the clock period of the input was 8 times of the sampling time. The period of the PRBS was 255. The outputs measured by INS, which includes gyro system, were attitude angles (Φ, Θ, Ψ), their angular velocities (p, q, r) and accelerations $(\dot{u}, \dot{v}, \dot{w})$. Velocities (u, v, w) and positions (x, y, z) were measured by GPS, and height (z) by a laser distance meter. The signals u, v and w, which

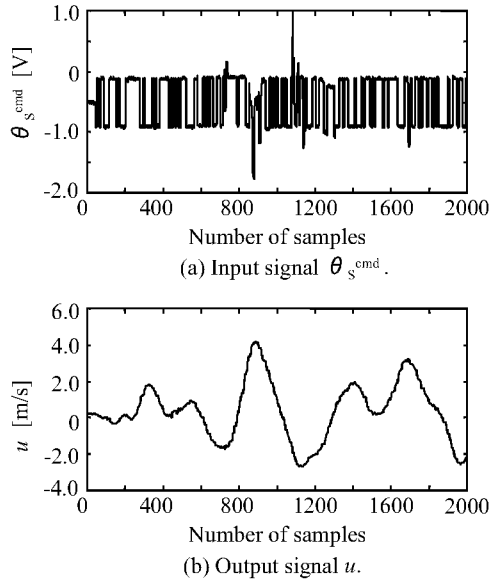

(a) Input signal θ_S^{cmd}.

(b) Output signal u.

Fig. 3. Input and output signals for pitch axis.

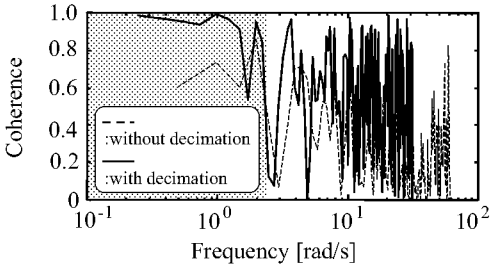

Fig. 4. Coherence for pitch excitation

directly influence the velocity control design for the autonomous flight, were selected as output signals for system identification.

As an example, the motion about pitching excitation is described below. The measured input and output signals are shown in Fig.3. As can be seen in Fig.3, it is verified that the output signal u, which is strongly related to a pitching motion, is excited by θ_S^{cmd}. The coherence between the input θ_S^{cmd} and the output u, which indicates how well θ_S^{cmd} corresponds to u at each frequency, is shown in Fig.4. The dashed line shows the coherence for the acquired input-output data. In order to improve the coherence in the lower frequency range which relates to the control band, the decimation filter (Vaidyanathan, 1993) consisting of the low pass filtering ($\pi/2$) and downsampling (0.1 s) is applied to the input-output data. The coherence for the decimated data is illustrated by the solid line. The accurate identification can be expected at the frequency range where the coherence is close to 1, which is shaded in Fig.4.

3.2 *System identification*

The system identification based on the prediction error method is applied to the decimated input-output data. The number of data was 1,000. The auto-regressive with exogenous input (ARX), auto-regressive moving average with exogenous input (ARMAX), output error (OE) and Box-Jenkins (BJ) models(Ljung, 1999) were used to describe the pitching dynamics of the helicopter. The cross-validation was utilized to determine the order of the ARX model, and then applied the order for the other models as well. Two thirds of the data were used for the identification, and the rest were used for validation. The model order that minimizes the loss function was the 23rd with two delays.

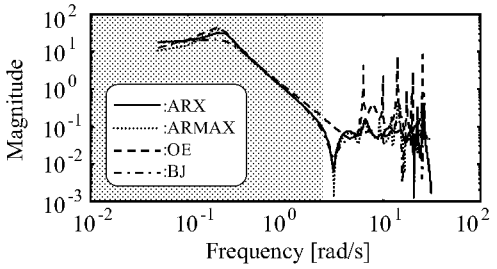

Fig. 5. Identified gain plots by various models for pitch excitation

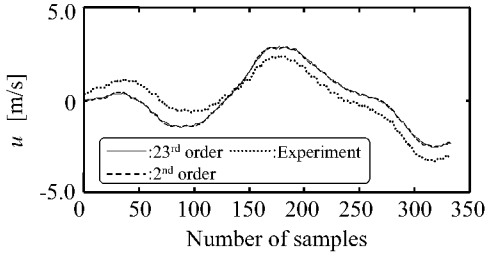

Fig. 6. Time responses of ARX model and reduced model to pitching excitation

Figure 5 shows identified gain plot from θ_S^{cmd} to the velocity u. As can be seen in Fig.5, the deviation among these four gain plots is small enough at the frequency range less than 3 rad/s, which falls in the range of a position control. Therefore, the frequency response of the pitching motion can be identified with high accuracy within the frequency range. It is also well known that the rigid body dynamics are dominant at that frequency range.

Next, to evaluate the identified model in time domain, the remaining one-third of input data were applied to the identified ARX model. From the viewpoint of dominant rigid body dynamics, the order of the identified model is reduced from the 23rd to the 2nd by means of the Gramian-based balancing method. Figure 6 shows time responses of these model outputs and the measured experimental output. It is confirmed by Fig.6 that the model outputs coincide with the measured output. Therefore, the identified and reduced models well describe the pitching motion of the experimental helicopter.

4. CONSTRUCTION OF GPS/INS HYBRID NAVIGATION SYSTEM

Information on the position of the body must be precisely acquired to realize the autonomous flight(M. Harigae and Shingu, 2000) of a large-scale unmanned helicopter. The sensors equipped with the body are the gyro, the accelerometer, the leaser altimeter and DGPS. It is difficult for a long time mission to use INS composed of the gyro and the accelerometer alone. Though, on the other hand, the sampling period of GPS is too long, it has the advantage of high precision for a long time. Therefore the authors construct the GPS/INS hybrid navigation system to introduce the advantages of GPS and INS.

The block diagram of the hybrid navigation system is shown in Fig.7. Kalman filter can be achieved by using the information from GPS and INS, whose sampling periods are 0.2 s and 0.05 s, respectively, using the following relationships. The measured acceleration for three directions is the sum of the acceleration of translation $\boldsymbol{a}$, the acceleration due to angular velocity $\omega \times \boldsymbol{u}$ where $\boldsymbol{u}$ is the velocity on the body, the bias $\boldsymbol{a}_b$, and the measurement error $\boldsymbol{v}_a$;

$$\boldsymbol{a}_m = \boldsymbol{a} + \omega \times \boldsymbol{u} + \boldsymbol{a}_b + \boldsymbol{v}_a \tag{1}$$

Velocities $\boldsymbol{U}_{E_m}$ and positions $\boldsymbol{X}_{E_m}$ on the earth which are measured by GPS also include the measurement errors $\boldsymbol{w}_{U_E}, \boldsymbol{w}_{X_E}$, respectively;

$$\boldsymbol{U}_{E_m} = \boldsymbol{U}_E + \boldsymbol{w}_{U_E} \tag{2}$$

$$\boldsymbol{X}_{E_m} = \boldsymbol{X}_E + \boldsymbol{w}_{X_E} \tag{3}$$

Relationship between the velocity on the body $\boldsymbol{u}$ and the velocity on the earth $\boldsymbol{U}_E$ with the gust $\boldsymbol{U}_g$ is;

$$\boldsymbol{U}_E = \boldsymbol{T}\boldsymbol{u} + \boldsymbol{U}_g \tag{4}$$

where $\boldsymbol{T}$ is a transformation matrix that relates the body to the earth.

The state-space equation for the Kalman filter is constructed with the state vectors $\boldsymbol{X}_E$, $\boldsymbol{U}_E$, $\boldsymbol{U}_g$ and $\boldsymbol{a}$. The output equation is constructed with the measured outputs $\boldsymbol{X}_E$ and $\boldsymbol{U}_E$. Observation update is done only when GPS data are measured.

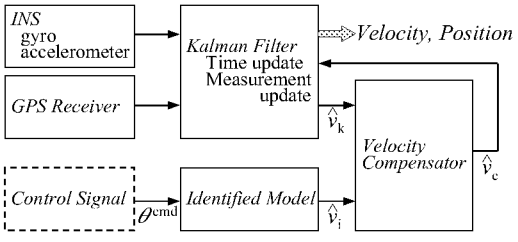

Fig. 7. Configuration of GPS/INS system

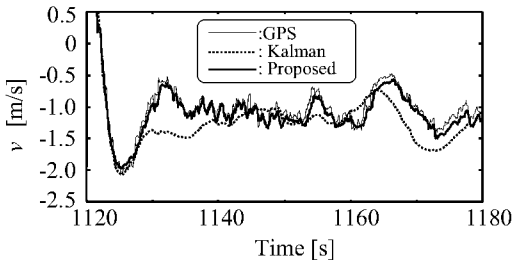

Fig. 8. Comparison between GPS and estimated data

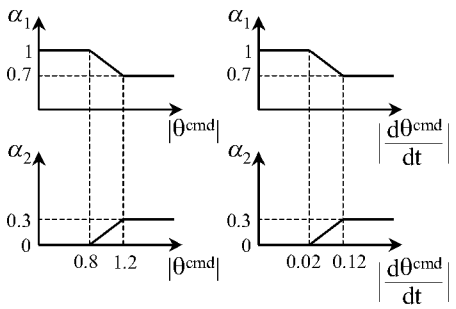

Fig. 9. Gain-scheduling weights to compensate estimation error

Time update can be accomplished after both INS and GPS data are acquired.

Simulations to estimate the position and velocity using actual experimental data were performed. Observed data of GPS and the estimated data are shown in Fig.8 by the thin line and the dotted line, respectively. Though estimated value agrees well with the slow movement, that does not follow the quick movement. This is the reason why the acceleration is assumed to be as the white noise in the above formula.

Now, the identified model described above is introduced to compensate the estimation errors. The estimated value derived from the identified model $\hat{v}_i$ is used with the estimated value from the filter $\hat{v}_k$ taking the size of control signal θ^{cmd} into consideration. The compensated value can be weighted according with

$$\hat{v}_c(t) = \alpha_1(\theta^{cmd})\hat{v}_k(t) + \alpha_2(\theta^{cmd})\hat{v}_i(t) \tag{5}$$

where $0 < \alpha_1 + \alpha_2 \leq 1$ and α is a function of θ^{cmd}. The considered gain-scheduling weights are presented in Fig.9. In this case, the authors also consider the rate of θ^{cmd}. The estimated value $\hat{v}_c$ compensated by this method is also shown in Fig.8 by the thick line. From this figure, it can be seen that the estimated value fits well with the quick movement.

Another aspect of this method will be the applicability of the same velocity information derived by using another information sources. Therefore, it can be directly applied to the diagnosis and so on.

5. POSITION CONTROLLER DESIGN

In this section, the design problem of position control system by using the identified model is focused. For the purpose of an autonomous flight, position control system with velocity feedback loop as minor control is recommended because the control system is subject to its flight modes. Fig.10 shows the block diagram of the position control system.

5.1 *Velocity control system*

In order to hold stability of the system against the model order reduction, the velocity controller is designed based on the $\mathcal{H}_\infty$ control theory(J. C. Doyle and Francis, 1989).

The design specifications for the velocity control are the followings;

(S1) There is no steady-state error to step reference.
(S2) Overshoot is as small as possible.
(S3) Settling time is less than 5 s.

The first and second specifications are defined relating to the accuracy of GPS. The third specification is defined from the viewpoint of the applied force which does not result in a mechanical damage somewhere in a body. In addition, the input signal θ^{cmd} is limited to ± 2 V.

In this design procedure concerning a pitching motion, it can be assumed that the model using the identified 23rd-order model (u/θ_S^{cmd}) shown in Fig.5 is the real experimental plant P, and the model using the reduced 2nd-order model is the nominal plant P_n. Figure 11 shows the gain plots of P and P_n. Then, the multiplicative uncertainty Δ_m, which is derived from $\Delta_m = (P - P_n)/P_n$, is shown in Fig.12. It is clear that the limitation of the bandwidth for the position control is less than 3 rad/s because of its zero-cross frequency. Taking limitation into account, the weighting function W_T for the complementary sensitivity function $T := PC_{vel}/(1 + PC_{vel})$, where C_{vel} is the controller transfer function, is selected to satisfy the restriction $|\Delta_m| < |W_T(j\omega)|, \forall\omega$, by

$$W_T(s) = \frac{s/0.1 + 1}{10} \tag{6}$$

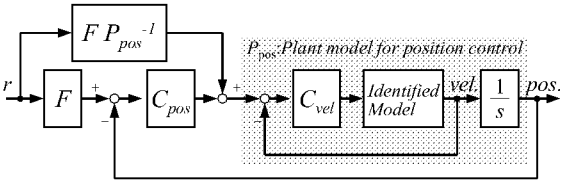

Fig. 10. Position control system

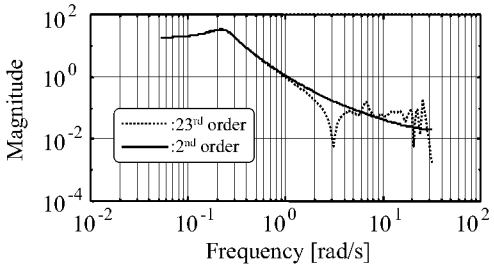

Fig. 11. Gain plots of P (solid line) and P_n (dotted line)

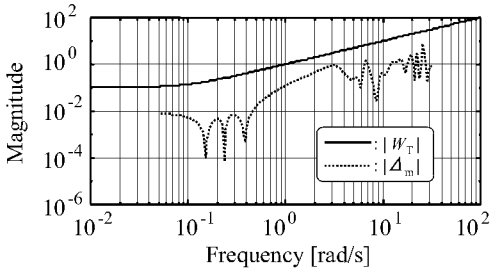

Fig. 12. Gain plots of Δ_m (dotted line) and W_T (solid line)

The gain plot is also shown by the solid line in Fig.12. In this design, the bandwidth is selected at 1 rad/s which can satisfy the specification (S3).

According to the weighting function W_S for the sensitivity function $S := 1/(1 + PC_{vel})$, it is recommended that W_S should be the integrator to satisfy the specifications (S1) and (S2) as the following, since its dynamics is directly reflected in the $\mathcal{H}_\infty$ controller.

$$W_S(s) = \frac{0.707}{s} \tag{7}$$

As a result of these weighting functions, the $\mathcal{H}_\infty$ controller of the 3rd-order can be obtained as

$$C_{vel}(s) = \frac{2.04 \times 10^3 (s + 0.075 \pm j0.247)}{s(s + 6.86)(s + 250)} \tag{8}$$

In order to examine the robust stability and the control performance of the system, a Boltzmann-shaped velocity reference, whose final value is 1 m/s and maximum gradient is 2 m/s^2, has been applied to the velocity control system. Figure 13 shows the time responses of the velocity u and the control input θ_S^{cmd}. In this figure, the dotted line shows the reference signal. The dashed line and solid line show the simulation and experimental results, respectively. Though the helicopter was strongly affected by the wind, the velocity settled into reference value.

5.2 *Position control system*

The design specifications for the position controller are almost the same as the specifications for the velocity controller except for the settling time

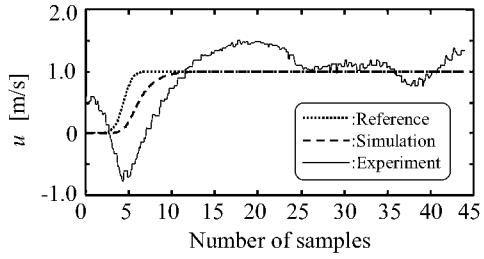

(a) Time responses of velocity u.

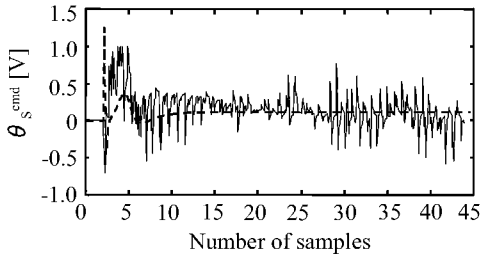

(b) Time responses of control input θ_S^{cmd}.

Fig. 13. Time responses to velocity reference

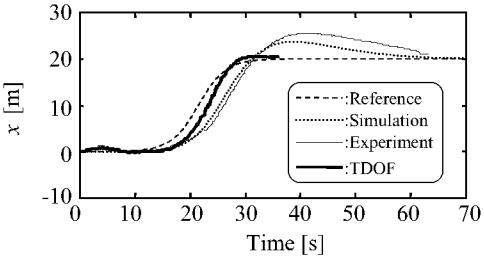

(a) Time responses of position x.

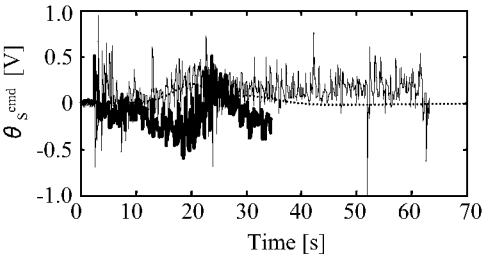

(b) Time responses of control input θ_S^{cmd}.

Fig. 14. Time responses to position reference

and overshoot. For position control system, the settling time is less than 15 s. From the viewpoint of simplicity of controller realization as well as no overshoot, in this case, two-degree of freedom (TDOF) control with PI position controller is utilized. The PI controller as illustrated below can satisfy the specifications for pitching movement.

$$C_{pos}(s) = \frac{14.3s + 1}{71.4s} \tag{9}$$

The rolling controller was designed by the same strategy. The position control experiment for the pitching has been carried out by using the above controller. The Boltzmann-shaped position reference with 20 m forward movement was applied to the pitching motion. Figure 14 shows time responses of the position and the control signal for one-degree-of-freedom control and TDOF control.

It can be concluded that the robust control can be performed by designed system not only to stabilize the system but also to follow the reference with the specifications satisfied.

6. CONCLUSION

System identification experiments were applied to the large-scale unmanned helicopter compensated by SAS. The modeling by system identification was established through numerical analysis using the measured data.

The authors have also focus on the construction method of the GPS/INS hybrid navigation system to derive the accurate aircraft's position.

Finally, the design procedure of robust position control system based on the TDOF control by introducing the identified model was proposed. The effectiveness of the proposed modeling and the design approach for an autonomous flight has been experimentally confirmed.

7. REFERENCES

G. Miyamori, Q. Zhao, M. Nakamura A. Tan K. Akachi and M. Hirai (1997). Development of an unmanned multipurpose utility helicopter(robocopter). *Proc. of 35th Aircraft Symposium of JSASS* pp. 89–92.

J. C. Doyle, K. Glover, P. P. Khargonekar and B. A. Francis (1989). State-space solutions to standard $\mathcal{H}_2$ and $\mathcal{H}_\infty$ control problems. *IEEE Trans. on Automatic Control* **34**, 831–847.

Kobayashi, Y. and K. Liu (1997). Modeling and robust control of a single-rotor helicopter (in japanese). *Proc. of SICE 26th Control Theory Symposium* pp. 111–116.

Ljung, L. (1999). *System Identification -Theory for the User (2nd edition).* Prentice Hall. New Jersey.

M. Harigae, T. Tsujii, M. Murata and H. Shingu (2000). *Development of Carrier-phase DGPS/INS Hybrid Navigation Algorithm (in Japanese).* Technical Report of National Aerospace Laboratory.

Nguyen, H. T. and N. R. Prasad (1999). *Fuzzy Modeling and Control -Selected Works of M. Sugeno.* CRC Press. London.

Vaidyanathan, P.P. (1993). *Multirate Systems and Filter Banks.* Prentice Hall. New Jersey.